Coastal Engineering 77 (2013) 108–119

Contents lists available at SciVerse ScienceDirect

Coastal Engineering

journal homepage: www.elsevier.com/locate/coastaleng

Prediction of waves generated by tropical cyclones with a quadtree-adaptive model

Chia-Cheng Tsai [a,*], Tien-Hung Hou [a], Stéphane Popinet [b], Yung Y. Chao [c]

[a] Department of Marine Environmental Engineering, National Kaohsiung Marine University, Kaohsiung, Taiwan
[b] National Institute of Water and Atmospheric Research, P.O. Box 14–901, Kilbirnie, Wellington, New Zealand
[c] Marine Modeling and Analysis Branch, NOAA Center for Weather & Climate Prediction, 5830 University Research Court, Room 2104, College Park, MD 20740, USA

ARTICLE INFO

Article history:
Received 30 August 2012
Received in revised form 29 January 2013
Accepted 25 February 2013
Available online xxxx

Keywords:
Quadtree
Wave spectral model
Hurricane Katrina
Hurricane Rita
Tropical cyclone

ABSTRACT

In this paper, we describe the application of a quadtree-adaptive model to hindcast the wave spectrum during Hurricanes Katrina and Rita. In the simulation, the quadtree grid system can be adapted to the vicinity of the hurricanes and/or some prescribed regions of interest, which require higher resolutions. In other words, the quadtree grid system can move with the hurricanes. Furthermore, all the details of prescribed simulations can be plugged into a global simulation with input wind fields at different resolutions. In addition, the prescribed model is implemented in a unified framework of code and performed in one thread or multiple parallel threads. The proposed adaptive model can significantly reduce the time required for a specific simulation and is very convenient for large-scale operational forecasting when multiple resolutions are required. For Hurricane Katrina, only 3 h of computing time is required to simulate the entire ten days of the hurricane event with a resolution of 0.25 h and 1/8 degree for the region of interest near Mexico bay. The difference between the predicted significant wave heights and the buoy measurements is less than 0.5 m. In addition, the codes of the models are freely available and thus can be easily extended to an operational forecast system of tropical cyclones.

1. Introduction

Many coastal, offshore and navigation engineering applications rely on a detailed wave climate at specific locations. However, such information is usually incomplete or even not available since in situ measurements are expensive. Therefore, an accurate and efficient prediction of wave conditions is crucial for these situations. For example, tropical cyclones out at sea or near coasts can cause high winds and result in large waves, which may disrupt international shipping, damage coastal structures and, sometime even cause shipwrecks.

Therefore, models for describing wave generation, dissipation and nonlinear wave–wave interactions are required. Tick (1959) first presented a nonlinear random model of gravity waves. Later, Phillips (1960) and Hasselmann (1960, 1962, 1963) almost simultaneously found the nonlinear energy transfer among wave spectral components which is caused by resonant four-wave interactions. After their developments, the wave action equation became the fundamental wind wave model for predicting large-scale ocean wave climate driven by wind-forced. A comprehensive review on the studies of ocean surface waves was given by Mitsuyasu (2002).

Then, Inoue (1967) and Barnett (1968) presented numerical implementations for the prescribed wind wave model. It should be mentioned, however, that a French group independently developed the numerical wave model in an earlier period (Gelci et al., 1957). After these pioneering works, several such models have been developed. These models are denoted as first, second or third generation wave models, depending on the level of parameterization of generation, dissipation and nonlinear wave–wave interactions. For example, the WAM (WAMDIG, 1988), WAVEWATCH (Tolman, 1991), and SWAN (Booij et al., 1999; Ris et al., 1999) are the better known third generation wave models used for computing wave spectra. The WAM code was originally developed for generating wave predictions in oceanic basins and deep water regions. Then, the current effect was added in the WAVEWATCH. On the other hand, the SWAN code was primarily focused on coastal regions.

Usually, the main focus of wave studies is on nearshore regions where a local high-resolution wave model should be applied with its boundary conditions obtained from lower-resolution models of a larger area. For example, Holthuijsen et al. (2000) upgraded the SWAN model by providing an option for coupling a low-resolution WAM and a high-resolution SWAN simulation. Lahoz and Albiach (1997) and Tolman (2008) have memtioned that the prescribed one-way nesting has some drawbacks. First, it is difficult to model the hurricane-induced swell traveling away to a lower-resolution region. Second, the one-way nesting is usually performed by a sequence

* Corresponding author. Tel./fax: +886 7 3617008.
E-mail address: tsaichiacheng@mail.nkmu.edu.tw (C.-C. Tsai).

0378-3839/$ – see front matter © 2013 Elsevier B.V. All rights reserved.
http://dx.doi.org/10.1016/j.coastaleng.2013.02.011

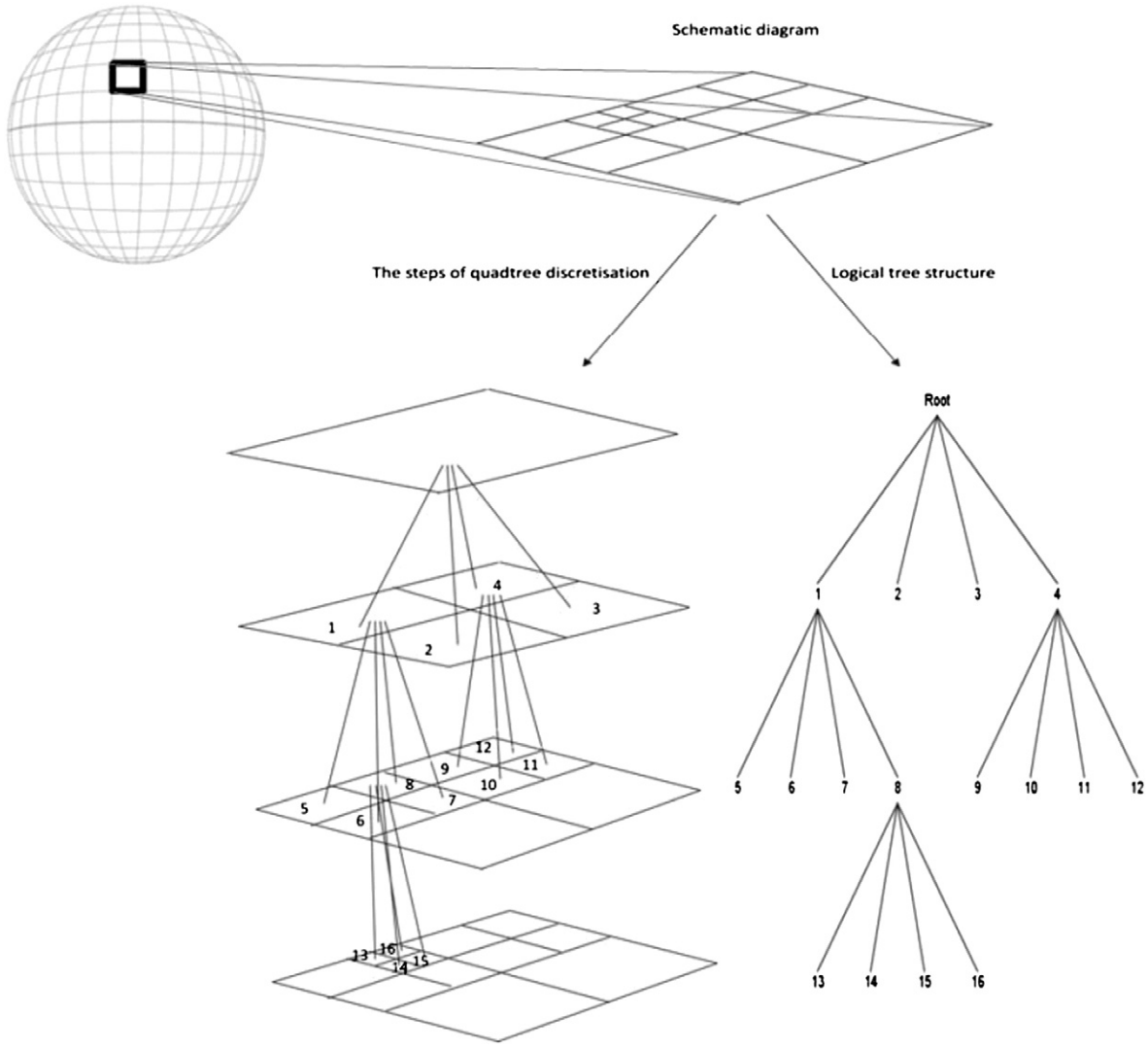

Fig. 1. Schematic diagram for the quadtree grid system.

of different threads which is not convenient for operational forecasting. Therefore, Tolman (2008) generalized the approach of Lahoz and Albiach (1997) and developed a two-way nested approach for wave modeling. In his approach, the area to be modeled was covered with mosaic grids with different resolutions. Each grid was considered as a separate wave model and two-way interactions are considered between all grids. In November 2007, his approach was implemented operationally at the National Centers for Environmental Prediction of USA (Chawla et al., 2007).

Alternately, there are also wind wave models using curvilinear or unstructured grids to adapt the resolution to areas of interest. For example, curvilinear grids were adopted in recent versions of the SWAN model (Booij et al., 1999; Ris et al., 1999). On the other hand, the finite element methods with unstructured spatial grids were also considered (Ardhuin et al., 2001; Benoit et al., 1996; Hsu et al., 2005; Liau et al., 2011).

However, only static grids are considered in all of these models. For hurricane applications, development of an approach with moving grids appears desirable. This was recently accomplished by Popinet et al. (2010), who integrated the source terms and spectral advection of WAVEWATCH version 3.14 (Tolman, 2009) into his quadtree-adaptive spatial solver of the finite volume method (FVM). The quadtree-adaptive FVM solver was originally designed for the dynamics of inviscid (Popinet, 2003) and viscous fluids (Popinet, 2009). The solver was also extended for solving shallow water equations (Popinet and Rickard, 2007) and applied to the modeling of the 2004 Indian ocean tsunami (Popinet, 2011) and the 2011 Japan tsunami (Popinet, 2012).

In the original study, Popinet et al. (2010) applied their quadtree-adaptive spectral wave model to an artificial hurricane. In the present study, the model is further applied to the 2005 Hurricanes Katrina and Rita. In the simulations, the quadtree grid system is adapted to the vicinity of the hurricanes and/or some prescribed regions of interest. Furthermore, we demonstrate how these simulations can be plugged into a global simulation with input wind fields of different resolutions. Therefore, the present quadtree-adaptive spectral wave model is very convenient and efficient for global operational forecasting when multiple resolutions are required.

2. Governing equations and numerical methods

In this study, we consider the wave spectra in water with zero mean currents which are described by the conservation of wave action (Bretherton and Garrett, 1968; Whitham, 1965) as

$$\frac{\partial N}{\partial t}+\frac{1}{\cos\phi}\frac{\partial\left(\dot{\phi}N\right)}{\partial\phi}+\frac{\partial\left(\dot{\lambda}N\right)}{\partial\lambda}+\frac{\partial\left(\dot{k}N\right)}{\partial k}+\frac{\partial\left(\dot{\theta}N\right)}{\partial\theta}=\frac{S}{\sigma} \tag{1}$$

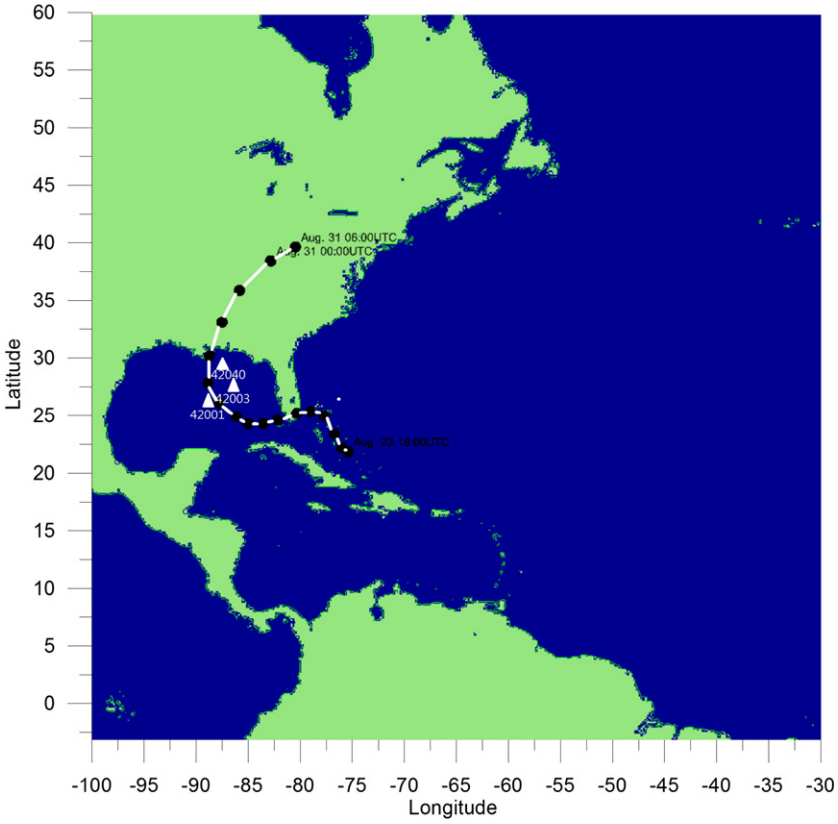

Fig. 2. The path of Hurricane Katrina.

Table 1
Buoy locations.

Bouy | Coordinates	Latitude	Longitude
42001	25.888 N	89.658 W
42003	26.044 N	85.612 W
42040	29.212 N	88.207 W

where the wave action is defined by

$$N(k,\theta,\phi,\lambda,t) = \frac{F(k,\theta,\phi,\lambda,t)}{\sigma} \tag{2}$$

with σ, k, θ, ϕ, λ and t being the radian frequency, the magnitude and direction of a wavenumber vector, the latitude, longitude and time coordinates respectively.

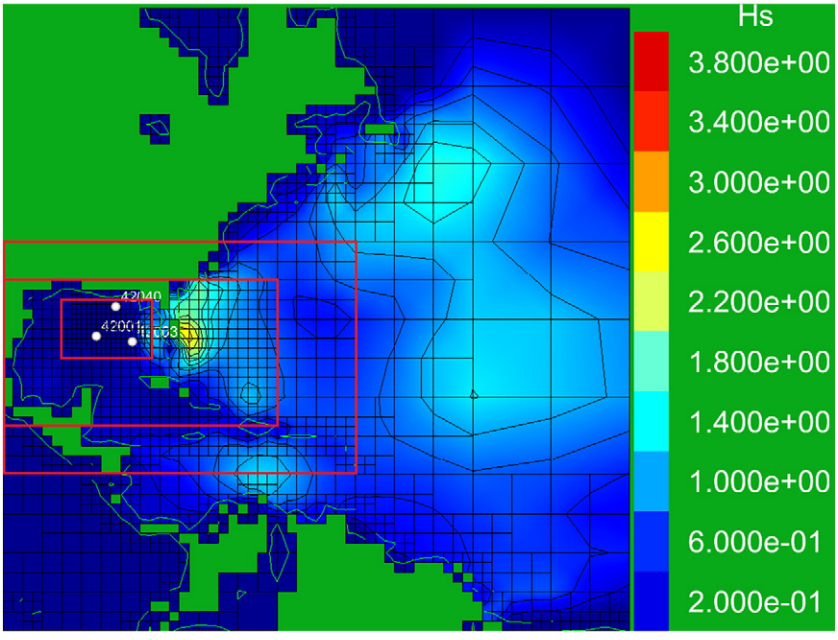

Fig. 3. A snapshot for simulating Hurricane Katrina by a static adaption model at August 26th 04:00 UTC.

Table 2
Variable-resolution information.

Level | Coordinates	Longitude	Latitude	Resolution (km)		
			Adaption 8	Adaption 7	Adaption 6
High	From 93°W to 84°W	From 24°N to 29.5°N	$7000/2^8$	$7000/2^7$	$7000/2^6$
Medium high	From 98°W to 75°W	From 16°N to 32°N	$7000/2^7$	$7000/2^6$	$7000/2^5$
Medium low	From 100°W to 60°W	From 15°N to 35°N	$7000/2^6$	$7000/2^5$	$7000/2^4$
Other	Elsewhere		Automatic		

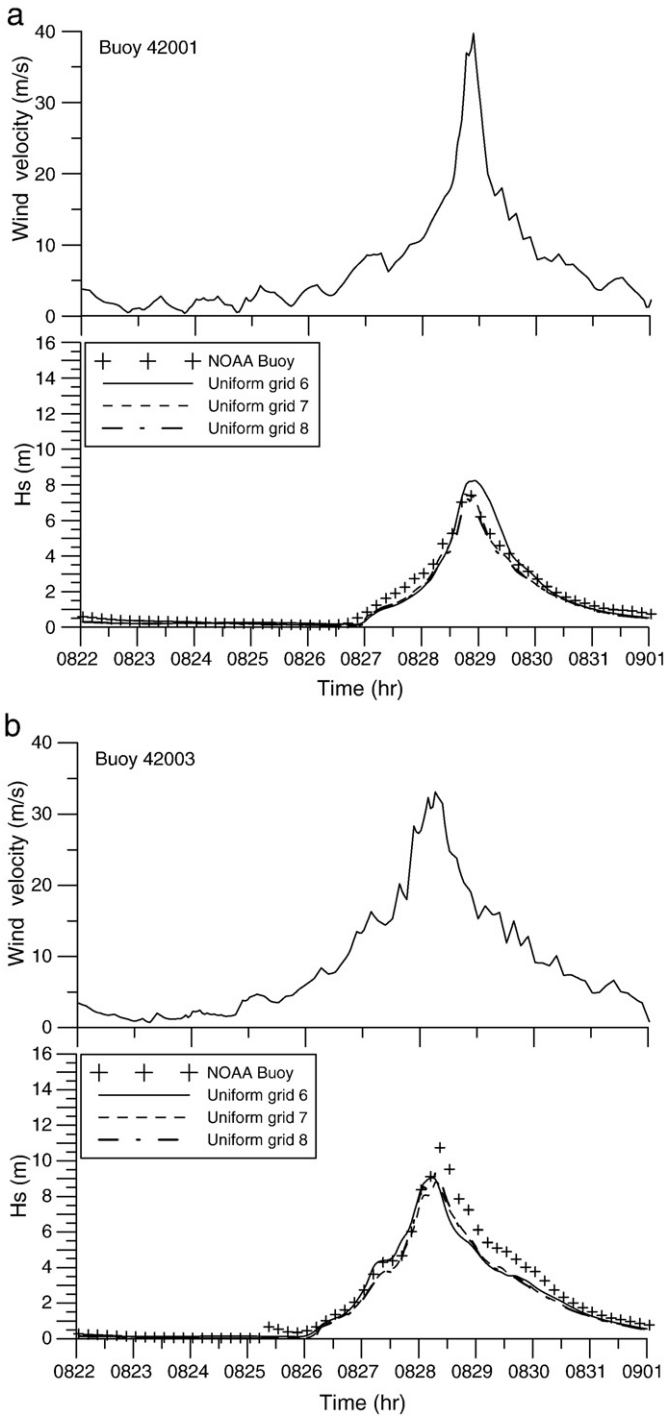

Fig. 4. Input wind field and comparisons of significant wave height time series by measurement and uniform-grid models at buoys (a) 42001, (b) 42003 and (c) 42040 for Hurricane Katrina.

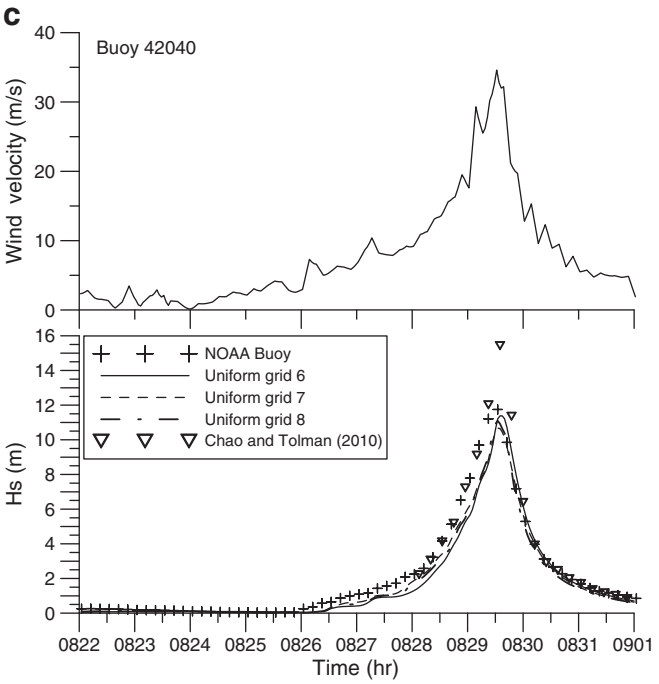

Fig. 4. (*continued*).

In addition, the net source term S in Eq. (1) is defined as

$$S = S_{\ln} + S_{nl} + S_{in} + S_{ds} + S_{bot} + S_{db} + S_{tr} + S_{sc} \tag{3}$$

where $S_{\ln}$ is a linear input term to provide more realistic initial wave field and S_{nl}, S_{in}, and S_{ds} are nonlinear wave–wave interaction, wind-wave interaction, and dissipation terms, respectively and are significant in deep water. In shallow water, additional source terms should be considered. In Eq. (3), S_{bot}, S_{db}, S_{tr}, and S_{sc} are wave–bottom interaction, depth-induced breaking, triad wave–wave interaction, and bottom-induced scattering terms, respectively. A more detailed introduction of these sources can be found in the user manual of WAVEWATCH.

In order to solve the action balance Eq. (1), a fractional step method (Hsu et al., 2005; Yanenko, 1971) is sequentially performed as follows

$$\frac{\partial N}{\partial t} + \frac{1}{\cos\phi}\frac{\partial\left(\dot{\phi}N\right)}{\partial\phi} + \frac{\partial\left(\dot{\lambda}N\right)}{\partial\lambda} = 0 \tag{4}$$

$$\frac{\partial N}{\partial t} + \frac{\partial\left(\dot{k}N\right)}{\partial k} + \frac{\partial\left(\dot{\theta}N\right)}{\partial\theta} = 0 \tag{5}$$

$$\frac{\partial N}{\partial t} = \frac{S}{\sigma} \tag{6}$$

The spatial advection Eq. (4) is solved in a spherical quadtree-adaptive grid as depicted in Fig. 1. In the solution procedure the advection terms in Eq. (4) is discretized at $t = (n + 1/2)\Delta t$ and treated by an upwind unsplit second-order Godunov algorithm, which was originally developed by Bell et al. (1989) for solving the incompressible Navier–Stokes equations in uniform grid system and extended to adaptive

Table 3
Numerical error, bias and computing time for Hurricane Katrina.

Hurricane Katrina								
Model type | Buoy	42001		42003		42040		Time (hr)	Speedup
	RMSE	Bias	RMSE	Bias	RMSE	Bias		
Uniform grid 6	0.47	–	0.75	–	0.74–	–	3.15	–
Uniform grid 7	0.28	–	0.68	–	0.58	–	8.79	–
Uniform grid 8	0.35	–	0.69	–	0.60	–	40.74	–
Static variable-resolutions 6	0.49	0.06	0.80	0.21	0.76	0.06	1.46	2.16
Static variable-resolutions 7	0.28	0.03	0.64	0.09	0.57	0.07	1.73	5.08
Static variable-resolutions 8	0.34	0.02	0.68	0.05	0.60	0.05	2.75	14.81
Dynamic adaption 6	0.48	0.03	0.75	0.04	0.76	0.05	1.49	2.11
Dynamic adaption 7	0.28	0.02	0.69	0.04	0.59	0.04	1.82	4.83
Dynamic adaption 8	0.36	0.02	0.70	0.04	0.62	0.05	3.09	13.18
Dynamic adaption 9	0.32	–	0.63	–	0.57	–	8.82	–
Chao and Tolman (2010)	0.53	–	−0.58	–	0.63	–	–	–

mesh refinement (AMR) and quadtree-adaptive grid systems by Martin and Colella (2000) and Popinet (2003), respectively. More details about the solution of the spatial advection can be found in the article of Popinet et al. (2010).

After the spatial advection is finished, C function calls are performed from the present quadtree-adaptive solver to the spectral advection and source reaction solvers implemented in Fortran in WAVEWATCH version 3.14 (Tolman, 2009).

For spectral advection, the solution is obtained by splitting Eq. (5) into wavenumber and directional advections which are sequentially solved by the ULTIMATE QUICKEST scheme (Leonard, 1979, 1991). Here, the ULTIMATE QUICKEST is simply a third-order upwind scheme with a limiter to avoid numerical extreme values. Finally, the source reaction (6) is solved by a semi-implicit integration scheme which was originally introduced in the WAM code (WAMDIG, 1988). Since these two stages are performed by WAVEWATCH, the corresponding parameters are specified using the WAVEWATCH input files. This completes a single time step and is sufficient for the time marching of the whole ocean wind wave model.

3. Numerical results

3.1. Static adaptive models to Hurricane Katrina

Hurricane Katrina is the costliest natural disaster and one of the five deadliest hurricanes in the history of the United States. Among recorded Atlantic hurricanes, it was the sixth strongest one overall and at least 1836 people died (Knabb et al., 2005).

When modeling the wave field produced by the Hurricane Katrina, we adopt the wind field used in the operational Western North Atlantic (WNA) wave model of the National Oceanic and Atmospheric Administration's (NOAA) WAVEWATCH III wave forecasting system. This wind field is obtained from the Global Forecast System (GFS) operated by the National Centers for Environmental Prediction (NCEP) (Moorthi et al., 2001). The GFS/WNA wind field is provided between latitude 0.25°S to 50.25°N and longitude 98.25°W to 29.75°W with a spatial resolution of 0.25° and a temporal resolution of three hours. To perform wind wave simulations, we consider a square computational domain of 7000 km with its center

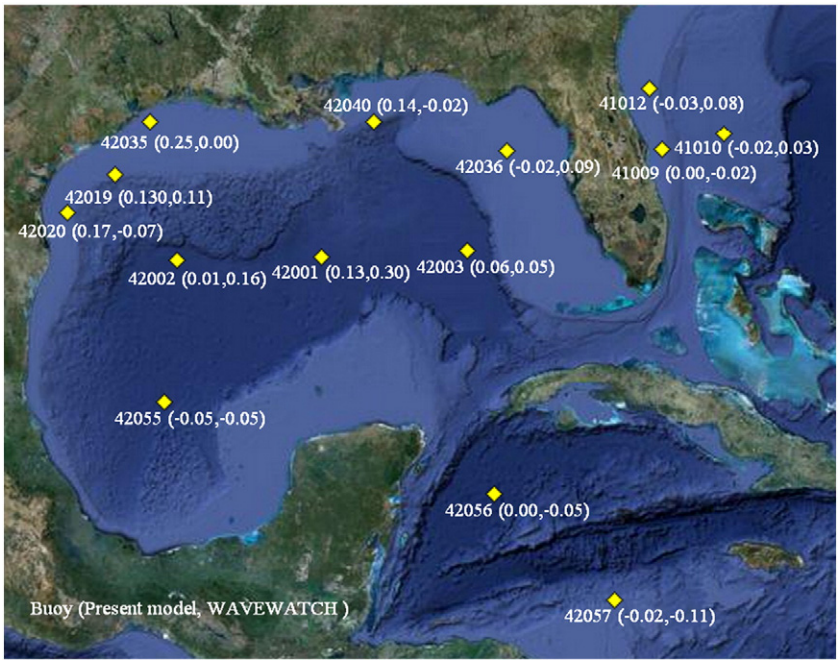

Fig. 5. RMSE improvements of high resolution over the low-resolution one for Hurricane Katrina.

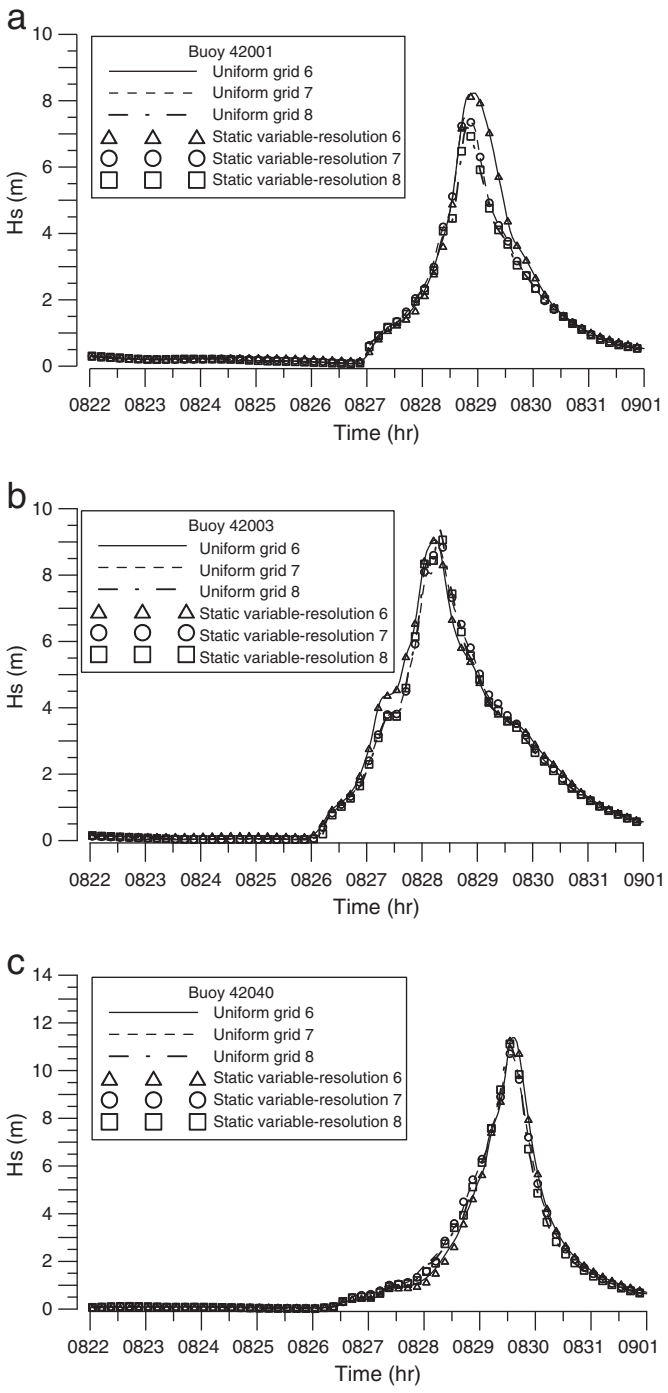

Fig. 6. Comparisons of significant wave height time series using static variable-resolution and uniform-grid models at buoys (a) 42001, (b) 42003 and (c) 42040 for Hurricane Katrina.

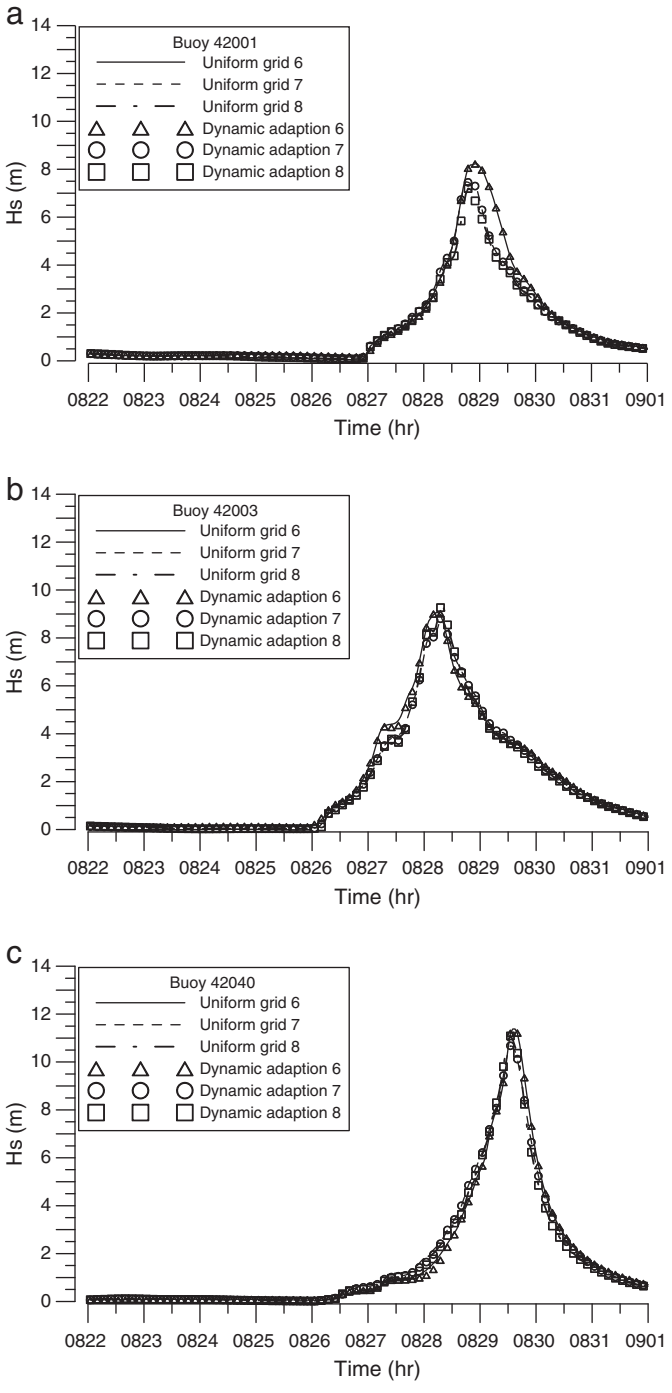

Fig. 7. Comparisons of significant wave height time series by dynamic quadtree-adaptive and uniform-grid models at buoys (a) 42001, (b) 42003 and (c) 42040 for Hurricane Katrina.

at latitude 30°N and longitude 65°W and the simulation time is a ten-days period from August 22nd 00:00 to September 1st 00:00 UTC. Clearly, this computational domain is larger than the domain of input wind field as depicted in Fig. 2. The initial condition is provided by a six-day warm-up simulation.

In order to perform static adaptive models, we consider an area of interest which requires a high resolution grid system defined between latitude 24°N to 29.5°N and longitude 93°W to 84°W. Inside this area, there are three buoy 42001, 42003, and 42040 as defined in Table 1. The high resolution area is enclosed by a medium high resolution grid system defined between latitude 16°N to 33°N and longitude 98°W to 75°W and a medium low resolution grid system defined between latitude 15°N to 35°N and longitude 100°W to 60°W. The resolution of the coast line is $7000/2^6$ km and the quadtree system of the rest area is at lower resolutions and is automatically arranged according the rule introduced in the article of Popinet (2003). Taking the 2^7 grid system as an example, a snapshot can be found in Fig. 3 with its high, medium high and medium low resolutions equal to 7000 km divided by 2^7, 2^6, and 2^5, respectively. In our numerical experiments, we consider three grid systems of variable-resolution

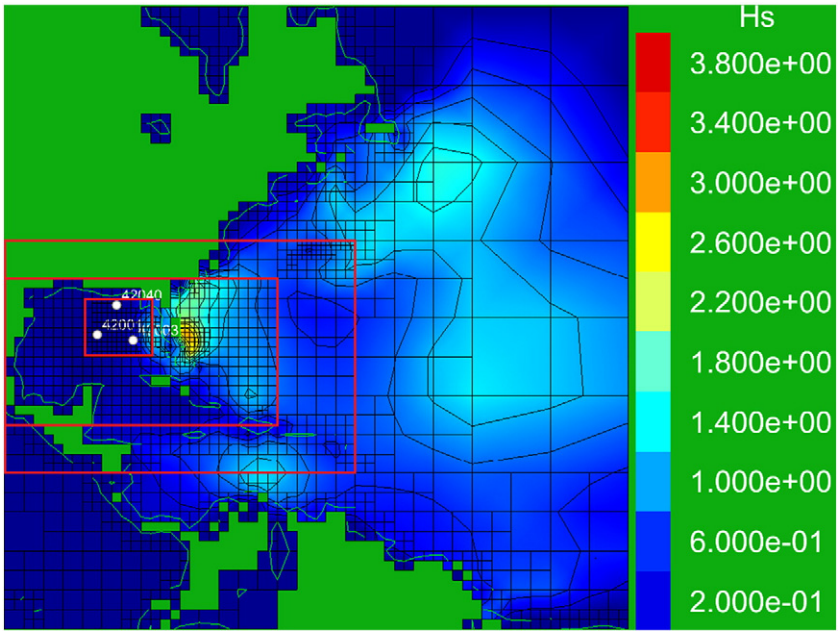

Fig. 8. A snapshot for simulating Hurricane Katrina by a dynamic adaption model at August 26th 04:00 UTC.

6, variable-resolution 7 and variable-resolution 8. Some details are given in Table 2. For comparison uniform grids of 2^6, 2^7, and 2^8 are also performed, whose spatial resolutions are about 1°, 0.5°, and 0.25° respectively.

Fig. 4 gives the comparisons between the measurements from the three buoys and numerical results on a uniform grid. In general, the numerical results are in very good agreement with the measurements from the three buoys. Table 3 gives the root mean

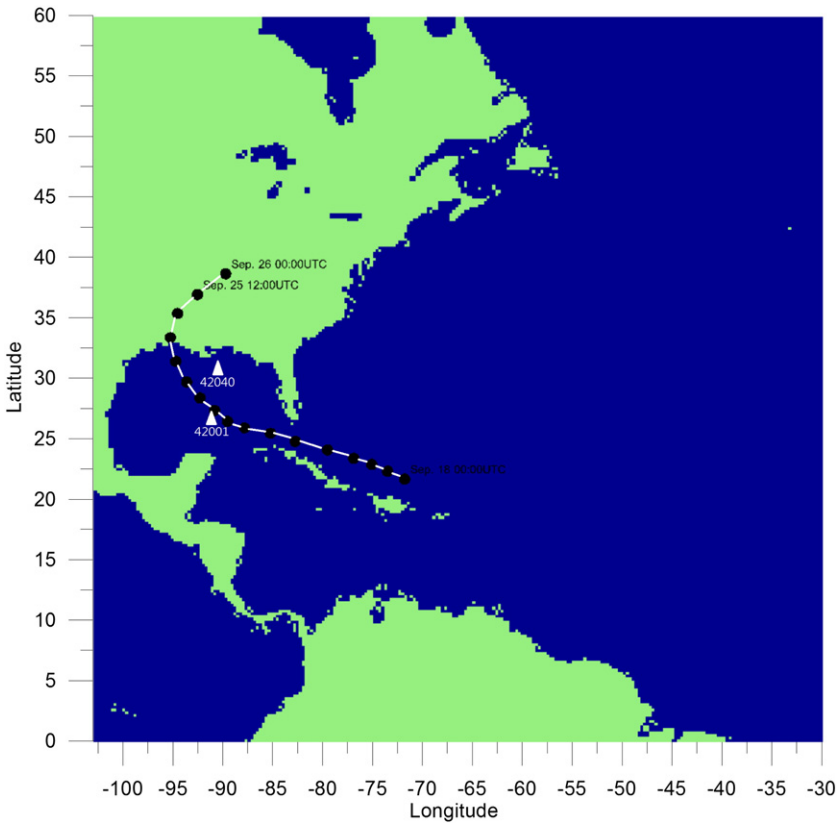

Fig. 9. The path of Hurricane Rita.

square error (RMSE) between the numerical results and the buoy measurements which are basically in the range 0.5–0.8 m, which is of similar level compared with the WAVEWATCH results obtained by Chao and Tolman (2010). This validates the constant-resolution model.

From Table 3, it can be observed that the RMSEs are only slightly improved from low to high resolutions. This is a common situation for wind wave prediction since the high-resolution input wind field of hurricane is also obtained by numerical models and thus always possesses uncertainty. Chao and Tolman (2010) have showed that two different wind fields can result in different wave heights while no one is significantly better than the other and at the same time these two wind fields are both different from the wind velocity of buoy measurements. In order to support this point, WAVEWATCH simulations are performed for spatial resolutions of 1° and 0.25°. The RMSE improvements of high resolution (2^8 or 0.25°) over the low-resolution one (2^6 or 1°) at different buoy locations are depicted in Fig. 5. In the figure, a better improvement can only be found for buoy 42040, which is just located on the continental slope.

Then we consider static variable-resolution models to save the computing time. In the studies, the bias is defined as the RMSE between the numerical result of a specific variable-resolution model and its corresponding uniform grid model. From Table 3, it is clear that the biases of the static variable-resolution models are basically very small. For a maximum resolution of 2^8, the biases are less than 0.08 m with a 14.81 speedup. To be clearer, the original computing for a uniform grid is 40.74 h and the corresponding static variable-resolution model requires only 2.75 h. However, the difference between their results is only about 0.08 m. Fig. 6 gives a comparison of the significant wave height time series obtained by the constant-resolution and variable-resolution models. The results of the two models are indeed very close.

3.2. Dynamic adaptive models to Hurricane Katrina

It is clear that the hurricane can produce large wind field. Therefore, a dynamic adaptive model seems natural for wind wave modeling of hurricanes. To demonstrate the dynamic adaptive model, we consider an adaption criteria where the resolution should stay high if the input wind field is larger than a certain threshold. In this study, the threshold is typically set as 12 m/s. For a model with a maximum resolution of 2^8, the high and medium resolution regions are set the same as the previous static variable-resolution models of 2^8 while an additional wind threshold is considered as described above.

As shown in Table 3, the biases of these dynamic adaptive models are further reduced when compared with the static variable-resolution models. And the additional computing time required for this dynamic adaption is limited as given in the table. Furthermore, Fig. 7 gives a comparison of significant wave height time series obtained by the models with uniform grids and dynamic adaption which are generally similar. Fig. 8 depicts a snapshot of the quadtree grid system at August 26th 04:00 UTC for the dynamic model. The adaption to the hurricane can be observed as compared to the corresponding static model shown in Fig. 3.

3.3. Hurricane Rita

The prescribed wind wave modeling can be easily extended to other hurricane events. Hurricane Rita was the fourth-most intense Atlantic hurricane ever recorded and the most intense tropical cyclone ever observed in the Gulf of Mexico (Knabb et al., 2006). In order to simulate the wave field of Hurricane Rita, we also use the GFS/WNA wind field for input and the computational domain is the same as those used in the previous examples. Models with uniform grids and dynamic quadtree adaption are considered. We have simulated the wave fields of Hurricane Rita in a nine-days period from September 17th 00:00 to September 26th 00:00 UTC. Similarly, the initial condition is provided by a six-days warm-up simulation. The path of Hurricane Rita can be found in Fig. 9.

Fig. 10 gives the wave height time series from buoy measurements and uniform grid modeling, which shows good agreements with each other. Fig. 11 gives a comparison of significant wave height

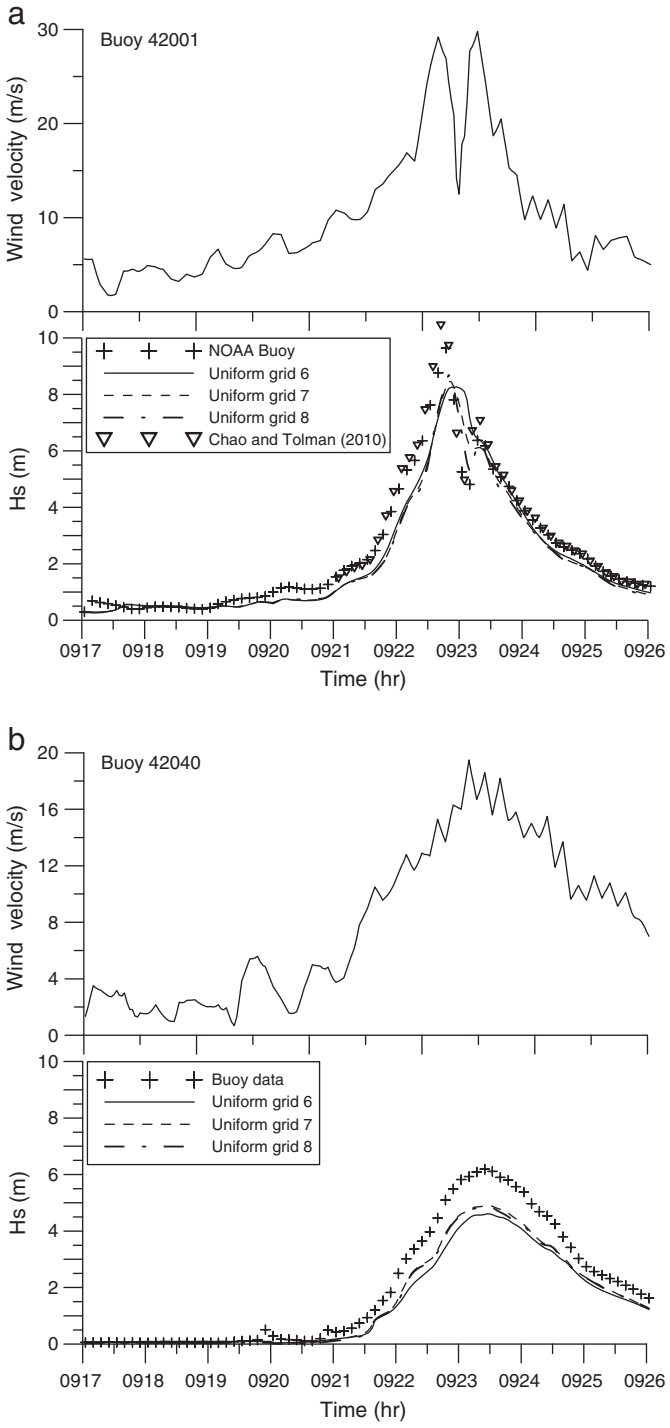

Fig. 10. Input wind field and comparisons of significant wave height time series by measurement and uniform-grid models at buoys (a) 42001 and (b) 42040 for Hurricane Rita.

time series obtained by the models with uniform grids and dynamic adaption, where it can be noticed that the results of the dynamic adaptive models are basically the same as their corresponding uniform grid models while the bias of the adaptive model from the uniform grid model is less than 0.06 m as given in Table 4. In addition, the results of both our models and WAVEWATCH (Chao and Tolman, 2010) have the RMSEs in the range of 0.5–0.85 m. The table also shows that the computing time for the dynamic adaptive model is reduced by a factor of 11.53 from that of the uniform grid model.

In Fig. 10(a), it can be observed form the data of buoy 42001 that there was a double-peaks wind velocity which resulted in a double-peaks wave heights. In our results, the double-peaks phenomenon is only significant for the simulation results of high-resolution models as shown in Fig. 12. In other words, only the high-resolution dynamic quadtree-adaptive model can hindcast the double-peaks significant wave height efficiently and accurately.

In addition, Fig. 13 gives snapshots of the quadtree grid system for both the dynamic model and its corresponding static one at September 21 10:00 UTC. In the figure, the adaption with respect to Hurricane Rita can be easily observed for the dynamic model. Overall, these results have demonstrated the feasibility of the present dynamic quadtree-adaptive model for simulating Hurricane Rita efficiently and accurately, especially for the double-peaks phenomenon.

3.4. Higher resolution

In Table 3, the computing time for the ten-day wind wave simulation of Hurricane Katrina in a uniform 2^8 by 2^8 grid is about 40 h. If a higher resolution (2^9 by 2^9) is required, the predicted computing time is about 40×4 h which is basically impractical for forecasting a ten-day hurricane event. A numerical test also resulted in a failure due to our limited memory storage for the case of this high resolution.

Table 4
Numerical error, bias and computing time for Hurricane Rita.

Hurricane Rita						
Model type | Buoy	42001		42040		Time (hr)	Speedup
	RMSE	Bias	RMSE	Bias		
Uniform grid 6	0.85	–	0.86	–	2.91	–
Uniform grid 7	0.79	–	0.68	–	8.19	–
Uniform grid 8	0.51	–	0.55	–	37.87	–
Dynamic adaptation 6	0.85	0.00	0.85	0.00	2.13	1.37
Dynamic adaptation 7	0.78	0.01	0.68	0.06	2.96	2.77
Dynamic adaptation 8	0.51	0.01	0.54	0.04	3.28	11.53
Chao and Tolman (2010)	0.78	–	0.34	–	–	–

However, the dynamic quadtree-adaptive model can be easily applied to this high resolution. We refine the model of dynamic adaption 8 to a model of dynamic adaption 9. In the model, the high resolution region and a moving area with input wind field larger than 12 m/s are resolved at about 13.7 kilometer ($7000/2^9$ km). The total computing time is about 8.82 h. Fig. 14 gives a snapshot of the dynamic quadtree grid system at August 26th 04:00 UTC. In the figure, the dynamic adaption can also be easily observed. Moreover, a comparison of significant wave height time series obtained by the models with dynamic adaption 8 and 9 are very close as depicted in Fig. 15. This has demonstrated that our dynamic quadtree-adaptive model can be easily extended to a higher resolution.

3.5. Full Atlantic model with two input wind fields

When applying the present quadtree adaptive models, it is not necessary to separate wind wave models to different regions even if the input wind fields have different resolutions. In addition to

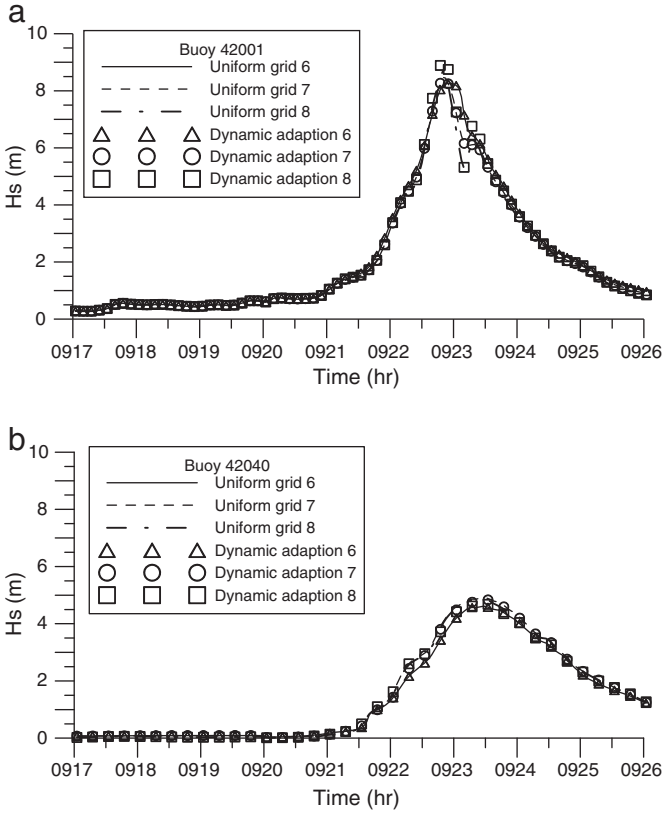

Fig. 11. Comparisons of significant wave height time series by dynamic quadtree-adaptive and uniform-grid models at buoys (a) 42001 and (b) 42040 for Hurricane Rita.

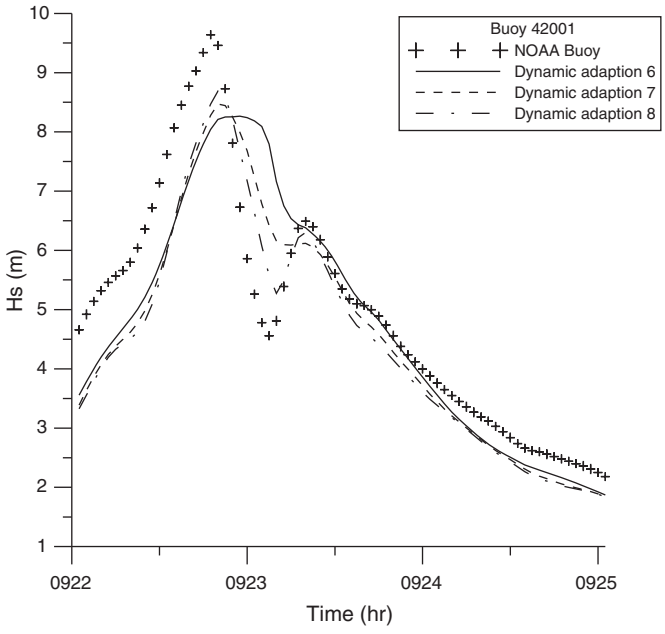

Fig. 12. Comparisons of double-peaks significant wave height for Hurricane Rita.

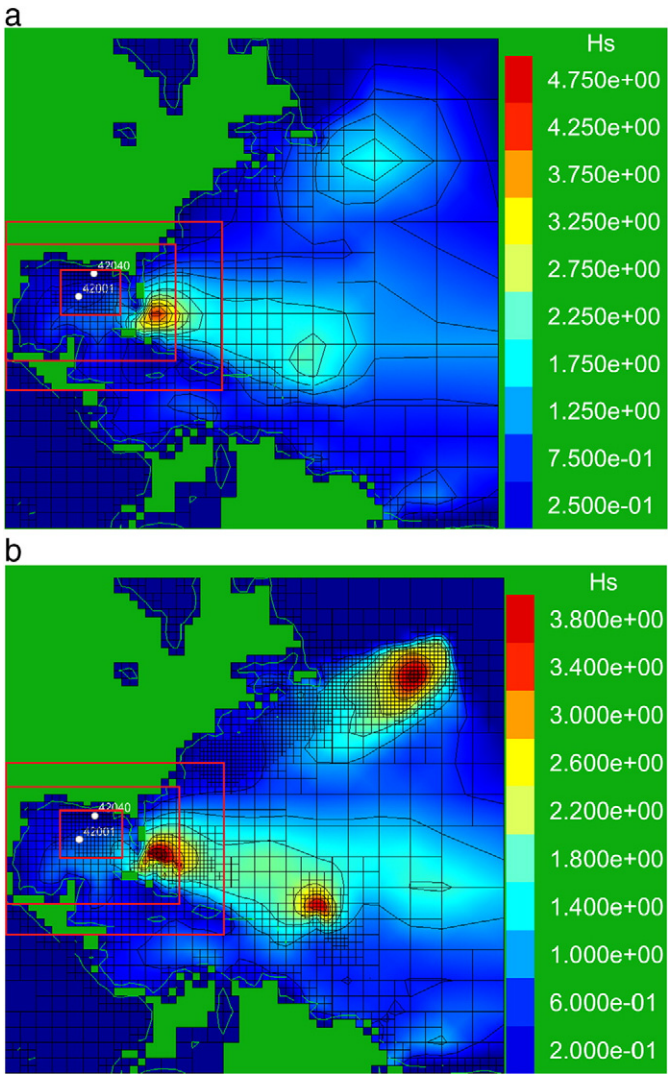

Fig. 13. A snapshot for simulating Hurricane Rita by (a) dynamic and (b) static adaption models at September 21 10:00 UTC.

the GFS/WNA wind field, NOAA also provides the GFS/30 arc-minute global grid(GLO_30m) wind field given between latitude from 77.5°S to 77.5°N and longitude from 179.5°W to 180°E with spatial resolution of 0.5° and temporal resolution of 3 h.

In order to demonstrate the applicability of the present quadtree adaptive model for two input wind fields, we simulate Hurricane Katrina in a square computational domain of 14,000 km with its center at latitude 25°N and longitude 27°W, which encloses the

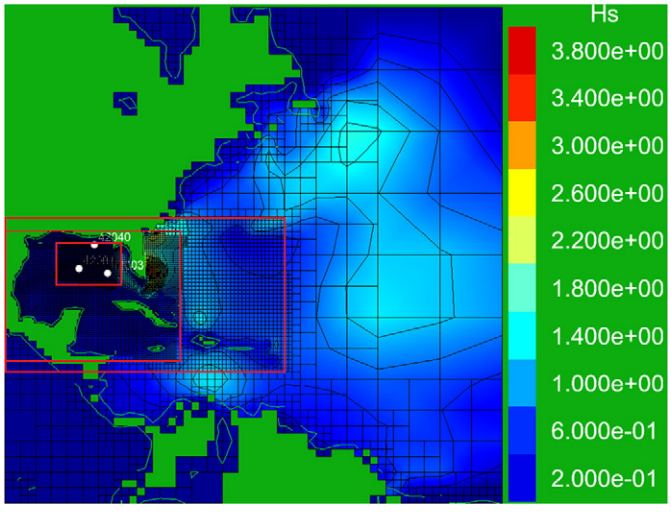

Fig. 14. A snapshot for simulating Hurricane Katrina by a dynamic adaption model of a higher resolution at August 26th 04:00 UTC.

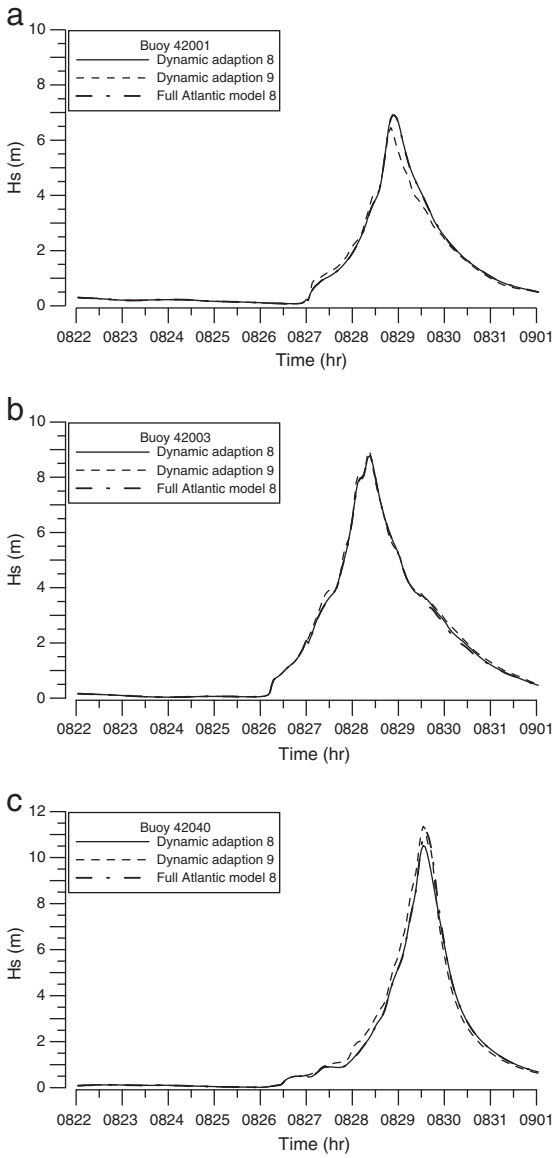

Fig. 15. Comparisons of significant wave height time series by dynamic quadtree-adaptive models of different resolutions and domains at buoys (a) 42001, (b) 42003 and (c) 42040 for Hurricane Katrina.

original computational domain and cover almost all the Atlantic ocean.

A dynamic adaption of 2^8 is performed. In other word, the high resolution area is set to $14{,}000/2^8$ kilometer, which is enclosed by a medium high resolution area of $14{,}000/2^7$ km and a medium low resolution area of $14{,}000/2^6$ km. Fig. 16 gives a snapshot of the dynamic quadtree grid system at August 26th 04:00 UTC, which nicely shows the dynamic quadtree adaptive characteristics. A comparison of significant wave height time series obtained by the present full Atlantic model and the previous local models are given in Fig. 15, which are in general agreement with each other. This has demonstrated that the present quadtree adaptive model can be applied to a more global ocean with two input wind fields.

4. Conclusion

A study on a dynamic quadtree-adaptive model for hindcasting the wave spectrum during Hurricanes Katrina and Rita was performed. Numerical results were compared with measurements from buoys, which showed good agreement. In addition, the numerical results of quadtree-adaptive and uniform-grid models were compared with each other. While the biases of simulated wave heights by the two models were limited to 10 cm, the computing times of the adaptive model were significantly reduced. In addition, wind-field criteria were set to make the quadtree grid system move with the simulated hurricane, which could provide a better simulation. For example, only the high-resolution dynamic quadtree-adaptive model can hindcast the double-peaks significant wave height efficiently and accurately at buoy 42001 during Hurricane Rita.

In a simulation for Hurricane Katrina, only 3 h of computing time was spent for simulating the ten-days event with a resolution of 0.25 h and 1/8 degree for the region of interest near Mexico bay. This result provided a speedup of a factor about 13 when compared with the computing time of the corresponding uniform-grid model. In addition, simulations at an even higher resolution and on a larger domain with two input wind fields were also performed and their results were also good. The source codes used are freely available online and are ready for a dynamic quadtree-adaptive modeling of other hurricane events.

Acknowledgement

The National Science Council of Taiwan under NSC 101-2628-E-022-001-MY2 is gratefully acknowledged for providing financial support to carry out the present work

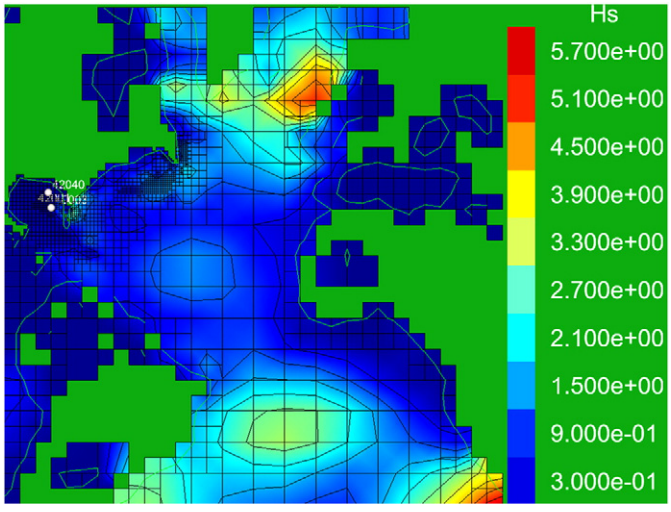

Fig. 16. A snapshot for simulating Hurricane Katrina by a dynamic adaption model covering almost the whole Atlantic ocean at August 26th 04:00 UTC.

References

Ardhuin, F., Herbers, T.H.C., O'Reilly, W., 2001. A hybrid Eulerian–Lagrangian model for spectral wave evolution with application to bottom friction on the continental shelf. Journal of Physical Oceanography 31 (6), 1498–1516.

Barnett, T.P., 1968. On the generation, dissipation, and prediction of ocean wind waves. Journal of Geophysical Research 73 (2), 513–529.

Bell, J.B., Colella, P., Glaz, H.M., 1989. A second-order projection method for the incompressible Navier–Stokes equations. Journal of Computational Physics 85 (2), 257–283.

Benoit, M., Marcos, F., Becq, F., 1996. Development of a third generation shallow-water wave model with unstructured spatial meshing. 25th International Coastal Engineering Conference, pp. 465–478.

Booij, N., Ris, R., Holthuijsen, L., 1999. A third-generation wave model for coastal regions. I — Model description and validation. Journal of Geophysical Research 104 (C4), 7649–7666.

Bretherton, F.P., Garrett, C.J.R., 1968. Wavetrains in inhomogeneous moving media. Proceedings of the Royal Society of London. Series A: Mathematical and Physical Sciences 302 (1471), 529–554.

Chao, Y.Y., Tolman, H.L., 2010. Performance of NCEP regional wave models in predicting peak sea states during the 2005 North Atlantic Hurricane Season*. Weather and Forecasting 25 (5), 1543–1567.

Chawla, A., et al., 2007. Operational Implementation of a Multi-grid Wave Forecasting System.

Gelci, R., Cazalé, H., Vassal, J., 1957. Prévision de la houle. La méthode des densités spectroangulaires. Bulletin d'Information du Comité d'Océanographie et d'Etude des Côtes 9, 416–435.

Hasselmann, K., 1960. Grundgleichungen der Seegangsvoraussage. Schiffstechnik 7 (39), 191–195.

Hasselmann, K., 1962. On the non-linear energy transfer in a gravity-wave spectrum. Journal of Fluid Mechanics 12 (481–500), 15.

Hasselmann, K., 1963. On the non-linear energy transfer in a gravity wave spectrum part 2. Conservation theorems; wave-particle analogy; irrevesibility. Journal of Fluid Mechanics 15 (02), 273–281.

Holthuijsen, L.H., et al., 2000. SWAN Cycle III version 40.11 user manual. Delft University of Technology Department of Civil Engineering, Netherlands.

Hsu, T.W., Ou, S.H., Liau, J.M., 2005. Hindcasting nearshore wind waves using a FEM code for SWAN. Coastal Engineering 52 (2), 177–195.

Inoue, T., 1967. On the growth of the spectrum of a wind generated sea according to a modified Miles–Phillips mechanism and its application to wave forecasting. DTIC Document.

Knabb, R.D., Rhome, J.R., Brown, D.P., National Hurricane, C., 2005. Tropical cyclone report: Hurricane Katrina, 23–30 August 2005. National Hurricane Center.

Knabb, R.D., Brown, D.P., Rhome, J.R., 2006. Tropical Cyclone Report, Hurricane Rita, 18–26 September 2005. National Hurricane Center, Miami.

Lahoz, M.G., Albiach, J.C.C., 1997. A two-way nesting procedure for the WAM model: application to the Spanish coast. Journal of Offshore Mechanics and Arctic Engineering 119, 20.

Leonard, B.P., 1979. A stable and accurate convective modelling procedure based on quadratic upstream interpolation. Computer Methods in Applied Mechanics and Engineering 19 (1), 59–98.

Leonard, B.P., 1991. The ULTIMATE conservative difference scheme applied to unsteady one-dimensional advection. Computer Methods in Applied Mechanics and Engineering 88 (1), 17–74.

Liau, J.M., Roland, A., Hsu, T.W., Ou, S.H., Li, Y.T., 2011. Wave refraction–diffraction effect in the wind wave model WWM. Coastal Engineering 58 (5), 429–443.

Martin, D.F., Colella, P., 2000. A cell-centered adaptive projection method for the incompressible Euler equations. Journal of Computational Physics 163 (2), 271–312.

Mitsuyasu, H., 2002. A historical note on the study of ocean surface waves. Journal of Oceanography 58 (1), 109–120.

Moorthi, S., Pan, H.L., Caplan, P., 2001. Changes to the 2001 NCEP operational MRF/AVN global analysis/forecast system. NWS Tech. Procedures Bulletin, 484 14.

Phillips, O.M., 1960. On the dynamics of unsteady gravity waves of finite amplitude Part 1. The elementary interactions. Journal of Fluid Mechanics 9 (02), 193–217.

Popinet, S., 2003. Gerris: a tree-based adaptive solver for the incompressible Euler equations in complex geometries. Journal of Computational Physics 190 (2), 572–600.

Popinet, S., 2009. An accurate adaptive solver for surface-tension-driven interfacial flows. Journal of Computational Physics 228 (16), 5838–5866.

Popinet, S., 2011. Quadtree-adaptive tsunami modelling. Ocean Dynamics 61 (9), 1261–1285.

Popinet, S., 2012. Adaptive modelling of long-distance wave propagation and fine-scale flooding during the Tohoku tsunami. Natural Hazards and Earth System Sciences 12 (4), 1213–1227.

Popinet, S., Rickard, G., 2007. A tree-based solver for adaptive ocean modelling. Ocean Modelling 16 (3), 224–249.

Popinet, S., Gorman, R.M., Rickard, G.J., Tolman, H.L., 2010. A quadtree-adaptive spectral wave model. Ocean Modelling 34 (1–2), 36–49.

Ris, R.C., Holthuijsen, L.H., Booij, N., 1999. A third-generation wave model for coastal regions 2. Verification. Journal of Geophysical Research 104 (C4), 7667–7681.

Tick, L.J., 1959. A non-linear random model of gravity waves I. Journal of Mathematics and Mechanics 8 (5), 643–651.

Tolman, H., 1991. A third-generation model for wind waves on slowly varying, unsteady, and inhomogeneous depths and currents. Journal of Physical Oceanography 21 (6), 782–797.

Tolman, H.L., 2008. A mosaic approach to wind wave modeling. Ocean Modelling 25 (1–2), 35–47.

Tolman, H.L., 2009. User manual and system documentation of WAVEWATCH-IIITM version 3.14. Technical note, MMAB Contribution(276).

WAMDIG, 1988. The WAM model—a third generation ocean wave prediction model. Journal of Physical Oceanography 18 (12), 1775–1810.

Whitham, G.B., 1965. A general approach to linear and non-linear dispersive waves using a Lagrangian. Journal of Fluid Mechanics 22 (02), 273–283.

Yanenko, N.N., 1971. The Method of Fractional Steps. Springer.